Yanbu Journal of Engineering and Science

Volume 22 | Issue 1 Article 8

2025

Effect of Al_2O_3 Passivation on Structured Si/PEDOT:PSS Hybrid Solar Cell

Sameer Alghanmi
Department of Mechanical Engineering, Jubail Industrial College, Royal Commission of Jubail, Jubail Industrial City, 31961, Saudi Arabia, ghanmis@rcjy.edu.sa

Khalid Alshammari
Department of Mechanical Engineering, Jubail Industrial College, Royal Commission of Jubail, Jubail Industrial City, 31961, Saudi Arabia, shammari_kd@rcjy.edu.sa

Follow this and additional works at: https://yjes.researchcommons.org/yjes
The journal in which this article appears is hosted on Digital Commons, an Elsevier platform.

Recommended Citation
Alghanmi, Sameer and Alshammari, Khalid (2025), Effect of Al_2O_3 Passivation on Structured Si/PEDOT:PSS Hybrid Solar Cell, *Yanbu Journal of Engineering and Science*: Vol. 22: Iss. 1, 84-91.
DOI: https://doi.org/10.53370/1658-5321.1196
Available at: https://yjes.researchcommons.org/yjes/vol22/iss1/8

This Research Article is brought to you for free and open access by Yanbu Journal of Engineering and Science. It has been accepted for inclusion in Yanbu Journal of Engineering and Science by an authorized editor of Yanbu Journal of Engineering and Science.

YANBU JOURNAL OF ENGINEERING AND SCIENCE 2025;22:84–91

Scan the QR to view the full-text article on the journal website

RESEARCH ARTICLE

Effect of Al_2O_3 Passivation on Structured Si/PEDOT:PSS Hybrid Solar Cell

Sameer Alghanmi *, **Khalid Alshammari**

Department of Mechanical Engineering, Jubail Industrial College, Royal Commission of Jubail, Jubail Industrial City, 31961, Saudi Arabia

ABSTRACT

Recently, silicon/organic heterojunction solar cells (HSCs) attain great attention because of its attractive characteristics such as rationally high efficiency, low cost, and simple device fabrication technique. However, inferior junction conformity between structured Si and PEDOT: PSS still remains a great challenge. Here, a superior, conformal, and uniform Al_2O_3 thin layer is deposited on structured pyramid n-Si wafer to enhance the front junction conformity using atomic layer deposition (ALD) technique. The deposited Al_2O_3 thin layer provides better wettability of PEDOT:PSS compared to native oxide, which minimizes pores, and pin-hole density usually occurs in spin-coating process. Additionally, Al_2O_3 thin layer acts as an electron-blocking and hole-transporting layer, resulting in an effective charge separation as well as transport, which boosts the power conversion efficiency. The interface-modified device demonstrates a high open-circuit voltage of 0.612 V as well as a fill factor of 70.7%, leading to a stable efficiency of 14.3% for structural n-Si/PEDOT: PSS HSCs.

Keywords: Silicon/organic heterojunction solar cells (HSCs), Structured silicon (Si), Atomic layer deposition (ALD), Spin-coating process, Electron blocking layer, PEDOT:PSS

1. Introduction

Silicon P-N junction solar cells are widely used because of their high power conversion efficiency (PEC), reliability, and stability, [1, 2]. However, complex fabrication process as well as high cost make silicon base solar cells quite complicated [3]. To minimize the complexity of fabrication as well as to reduce the cost, recently Si/PEDOT: PSS HSCs have been widely studied because of their attractive characteristics such as low-temperature fabrication method, simple device structures, rational light-trapping ability, and cost-effectiveness [4, 5]. Facile spin coating method of PEDOT:PSS form a heterojunction with n-Si imparting an effective level of passivation, and an inversion layer additionally, the performance of HSCs change by varying the thickness of PEDOT:PSS [6–10]. However, the PCE of Si/PEDOT:PSS HSCs are primarily limited as a result of inferior junction quality at the front interface between n-Si and PEDOT:PSS [11–13]. To improve the performance of the front interface several groups utilized different techniques to effectively enhance the junction quality [14–17]. Among these techniques, a facile and simple method is the utilization of surfactant such as p-t-octyl phenol (Triton X-100) [18], and fluorosurfactant Zonyl FS-300 [19], added in PEDOT:PSS solution which enhances the junction quality. Although the use of surfactants effectively enhances junction quality, it impairs the conductivity of PEDOT:PSS and results in unsatisfactory junction formation, which deteriorates the overall performance of the device [20]. Another frequently utilized technique to improve front interface quality is converting the hydrogen-terminated Si surface to an oxygen-terminated Si surface. The formation of SiO_x-Si bonds creates a favorable band alignment between Si and PEDOT, promoting

Received 20 November 2024; accepted 1 December 2024.
Available online 1 June 2025

* Corresponding author.
E-mail addresses: ghanmis@rcjy.edu.sa (S. Alghanmi), shammari_kd@rcjy.edu.sa (K. Alshammari).

https://doi.org/10.53370/1658-5321.1196
1658-5321/© 2025 The Author(s). Yanbu Journal of Engineering and Science. This is an open access article under the CC BY 4.0 Licence (https://creativecommons.org/licenses/by/4.0/).
Published by Yanbu Industrial College, Saudi Arabia. The journal is hosted on Digital Commons, an Elsevier Platform.

effective charge separation [21, 22]. However, delicate adjustments in surface topology, hydrophilicity, and oxide thickness can lead to discrepancies in PCEs because SiO_x quality is normally very sensitive to environmental conditions, such as humidity, temperature, and oxygen. Another technique frequently utilized to improve the performance of HSCs is the application of a thin layer that acts as both a light absorber and a barrier for charge carriers [23–25]. Similarly, Sheng *et al.,* treated Si wafers with HNO_3 and H_2O_2 solution which effectively enhanced the junction between Si and PEDOT:PSS [26]. Similarly, Chen *et al.,* used a diluted NaOH solution to improve the front interface of HSCs [27]. Although the use of acids, oxidizing agents, dilute NaOH, and other solution treatments enhances junction quality, their corrosive nature, harmful effects, and unsatisfactory interfacial layer formation limit practical application. Additionally, Liu *et al.,* utilized TiO_2 for rear interface modification using a solution technique [28]. However, controlling layer thickness, composition, and distribution of depositing material using these methods can be challenging, impacting the separation, and transport of photo-generated charge carriers. To mitigate these disadvantages and further improve the junction quality between structured Si and PEDOT, additional research is needed to explore effective strategies for boosting the PCE. ALD has been found promising due to its advantages of self-limiting nature over other physical or chemical deposition techniques, such as electroplating, spin coating, sputtering, physical vapor deposition and chemical vapor deposition [29, 30].

In this work, we employed atomic layer deposition (ALD) to deposit a conformal, uniform, and ultrathin layer of Al_2O_3 on structured Si with a high aspect ratio and angstrom-level precision. Compared to conventional SiO_x interfaces, the ALD-deposited layer demonstrates enhanced PCE, mainly due to the suppression of photogenerated charge carriers and improved surface wettability. Additionally, the ALD-deposited Al_2O_3 thin layer perform both the function of passivation, and recombination barrier layer. The effect of ultrathin Al_2O_3 layer and its effects on the performance of HSCs, were studied via current density–voltage (J–V) plots, electrochemical impedance spectroscopy (EIS), and external quantum efficiency (EQE) measurements.

2. Experimental section

Single-side polished Phosphorus doped n-type Si wafer with a resistivity of 1–3 Ω cm, Czochralski (CZ), and thickness (520 ± 20 μm) possessing (an active area of 1 × 1 cm^2) was used in device fabrication. Before Al_2O_3 deposition, the Si wafers were first cleaned with standard RCA procedure. To synthesize the pyramid structure, we utilized the optimized condition reported by Li *et al.,* and Sharma *et al.,* the Si wafer were treated in a bath that contain with a dilute mixture of isopropyl alcohol and potassium hydroxide at concentrations of 0.1 M and 0.5 M, respectively, for 45 minutes at 75 °C, followed by rinsing and drying [31, 32]. While the rear surface was kept intact and protected by Miccroshield Stop-Off Lacquer by Tolber. Subsequently, a thermal reactor (CN-1 Co., Atomic Classic) ALD was utilized to deposit ultra-thin Al_2O_3 on structured pyramid Si. Triethylaluminium (TMA) and H_2O were used as the reactant precursors during the Al_2O_3 deposition process. The injection time for H_2O and TMA was 100 and 200 ms respectively, for individual ALD cycle, followed by 10 s of purging with N_2. A single cycle of the ALD technique was sequenced as TMA pulse, lodging, N_2 purging, H_2O pulse, lodging, and N_2 purge. Next, PEDOT:PSS (PH1000) solution was spin-coated on the front interface of structured Si for 60 s at 2500 rpm followed by annealing process resulting in a highly conductive p-type thin film of ~120 nm [33]. Finally, 300 nm Al thin layer and Ag grid were deposited on rear and front interfaces respectively using thermal evaporator.

2.1. Characterization

The surface chemical composition of the Al_2O_3 deposited structured Si was evaluated by using XPS (Thermo-VG Scientific ESCALAB 250. Scanning Electron Microscope (SEM, SU5000, HITACHI) was used to study high-resolution images of structured pyramids. Different Al_2O_3 thickness was determined using a spectroscopic ellipsometer (SE, MG-1000, Nano-view).

2.2. Photovoltaic properties measurements

The Photovoltaic (PV) characteristics were evaluated using a solar simulator (Peccel PEC-L11) at air mass (AM) 1.5 G (100 m W/cm^2 illumination). The EQE was measured at a beam size of 1 × 1 mm^2 using a xenon monochromatic light source in the wavelength range of 350–1100 nm. Optical reflection was measured using a spectrophotometer (Lambda 750, PerkinElmer) in the wavelength range of 350–1100 nm.

3. Results and discussion

Structured pyramid Si/PEDOT:PSS HSCs were fabricated by the route as revealed in Fig. 1. Different steps are involved in the fabrication of HSCs, such as

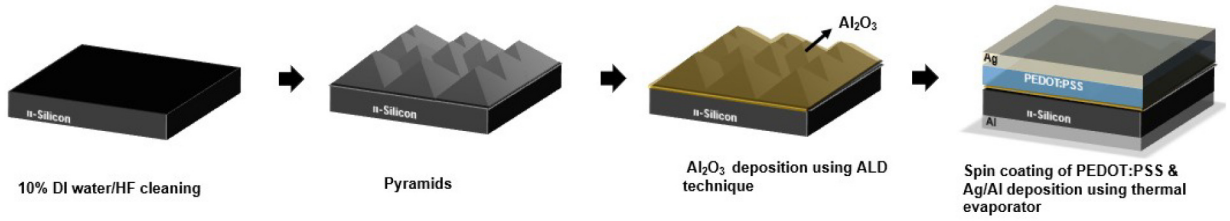

Fig. 1. Schematic demonstrating the fabrication of structured n-Si/PEDOT: PSS HSCs.

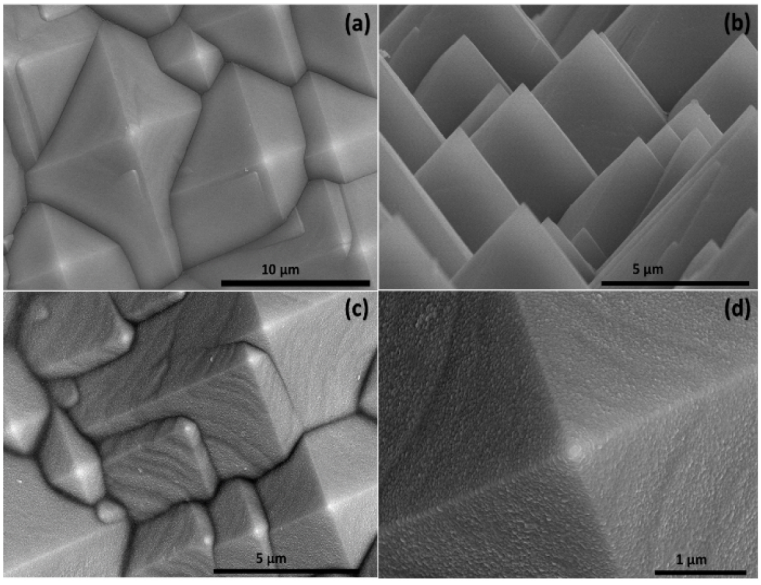

Fig. 2. SEM images demonstrating (a) top as well as (b) cross-section view of synthesized pyramid structure without PEDOT:PSS deposition, while (c) demonstrating top view at low and (d) high magnification after PEDOT:PSS deposition.

etching, Al_2O_3 deposition, PEDOT:PSS coating, and Ag/Al electrode deposition. Furthermore, Fig. 2a-b, demonstrate the top as well as a cross-sectional view of synthesized pyramids without PEDOT:PSS deposition. Pyramids of sizes 5∼10 μm can be seen in Fig. 2a. A large-scale silicon pyramid array with a uniform size distribution was successfully prepared on the surface of a silicon wafer, exhibiting strong anti-reflection properties. This improved anti-reflection capability, in turn, enhances the current density of HSCs. Furthermore, the valleys of the synthesized pyramids are fully covered with PEDOT:PSS at low magnification as shown in Fig. 2c. While, Fig. 2d represent the successful as well as conformal deposition of PEDOT:PSS on high magnification. The uniform and conformal coverage of PEDOT:PSS on structured pyramid resulted mainly due to ultra-thin Al_2O_3 deposition. These conformal junction between the PEDOT:PSS and structured pyramid resulted in effective charge separation as well as migration which boost the photovoltaic performance. To further evaluate the successful deposition of Al_2O_3 thin layer on structured Si, XPS

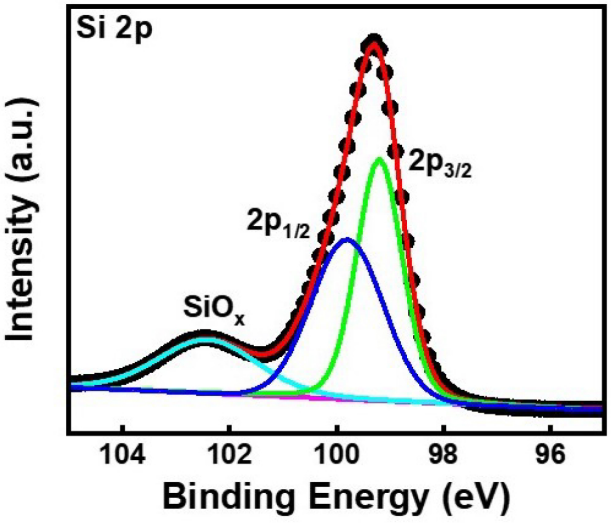

Fig. 3. XPS analysis of Si (2p) with Al_2O_3 deposited on pyramid Si structure.

analysis was done as shown in Fig. 3. In survey spectrum, the peaks of individual components can be seen which indicate the successful deposition of Al_2O_3 thin

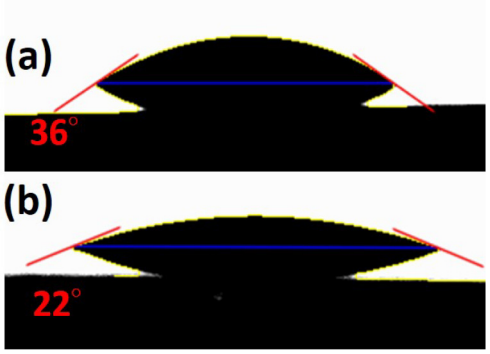

Fig. 4. Contact angle measurements with a water drop for (a) native oxide, and (b) with Al_2O_3.

layer on a structured Si along with Al and O core level spectra [34]. Furthermore, Si 2p core level spectrum (Fig. 3) can be split into two prominent peaks e.g., $2p_{1/2}$ and $2p_{3/2}$ due to spin-orbit coupling, with an additional SiO_x peak at 102.5 eV. Additionally, core level spectra of Si 2p demonstrate the presence of Si(0) and Si(4^+) states at their respective binding energy position [35]. The peak at 102.5 eV specifies the oxidation of structured Si wafer generating a SiO_x layer during Al_2O_3 deposition [36].

To evaluate the wettability of PEDOT: PSS with and without Al_2O_3 deposition contact angles (θ) were measured, which are 36° and 22° for native oxide and Al_2O_3 respectively. The Al_2O_3 thin layer deposited on front surface can enhance the surface energy, which generates the uniform coating of PEDOT:PSS, acting as an electron blocking layer. Lower contact angle indicates higher wettability of PEDOT: PSS solution on structured Si surface allows the uniform and conformal junction formation. This minimizes the defects such as pores, cracks, and micro voids which frequently occur during the spin-coating process, these cracks and pores act as a recombination center for photogenerated charge carriers as revealed in EIS data (Fig. 6b) the interface modified HSCs demonstrate effective photogenerated charge carriers separation and migration compare to pristine [37].

Table 1. Photovoltaic characteristics of the HSCs with and without interface modification.

Devices	V_{oc} (V)	J_{sc} (mA/cm^2)	FF (%)	PEC (%)
Al_2O_3 Treatment	0.612	33.1	70.7	14.3
Native Oxide	0.587	32.1	65.9	12.4

To evaluate the role of optimum layer thickness on HSCs performance we deposited different layers of Al_2O_3 utilizing ALD technique. Among different layers 2 nm thin layer of Al_2O_3 performs best photovoltaic performance mainly due to active passivation, electron blocking and hole transporting mechanism. A decrease in Al_2O_3 thickness resulted in poor performance mainly due to insufficient passivation while increasing the thickness beyond 2 nm blocks the tunnelling of holes, dramatically decrease FF, and increase series resistance all these factors impede the PCE of HSCs [38]. Furthermore, the current density-voltage (J-V) characteristic (Fig. 5a) of both devices were compared while Table 1 represents the output photovoltaic characteristics. Enhanced photovoltaic performance directly related with effective passivation at the front junction between structured Si and PEDOT:PSS. Additionally, Fig. 5b presents the dark-current density versus voltage (J0J_0J0–VVV) characteristics for both the modified and native oxide devices. The interface modified device demonstrate lower J_0 compared to pristine mainly due to effective passivation resulting from Al_2O_3 deposition [39, 40]. Effective passivation resulted in lower (J_0) value which in turn enhanced the FF and V_{oc} of device due to its inverse relation given by the following equation [31, 41].

$$V_{oc} = \frac{nkT}{q} ln \frac{J_{sc}}{J_0} \quad (1)$$

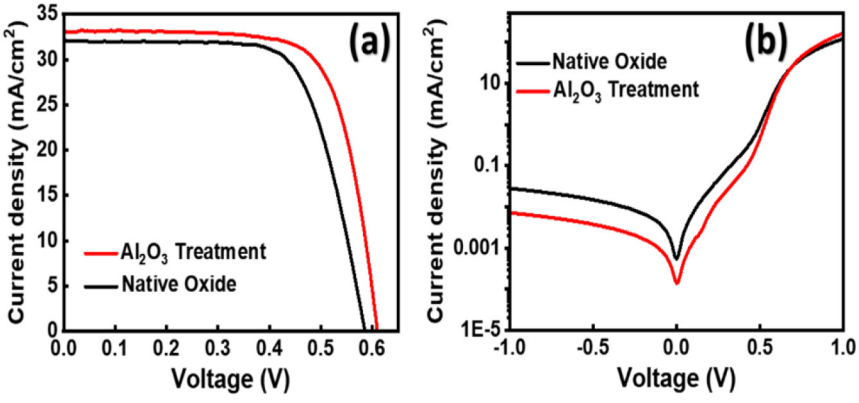

Fig. 5. (a) I-V characteristic of the devices under light (b) J_0-V characteristic of the devices under dark.

Table 2. (J_0), (n) and (Φ_b) parameters of structured Si/PEDOT:PSS HSCs with and without interface modification obtained from dark J–V curves.

Devices	J_0 (A/cm^2)	Φ_b (eV)	n
Native Oxide	5.3×10^{-7}	0.802	2.14
Al_2O_3 Treatment	1.3×10^{-7}	0.843	1.92

where k is the Boltzmann constant, T represent temperature, q is the electric charge, n is the ideality factor. The value of n is different for pristine and interface modified devices. Higher n value demonstrates a higher charge recombination rate and vice versa, as shown in Table 2 interface modified device demonstrating small value of n indicating enhanced photogenerated charge transfer mechanism. Additionally, from value of J_0, the Schottky barrier height (Φ_b) can be calculated by using the equation [7, 42, 43].

$$V_{oc} = A^*AT^2\exp\left(-\frac{\Phi_b}{kT}\right) \quad (2)$$

In Eq. (2), J_o represent reverse saturation current density, A represent active area, A* is the active Richardson constant, T denote absolute temperature, Φ_b represents the Schottky barrier height and k is the Boltzmann constant. The interface modified device demonstrates higher Φ_b 0.843 value compare to 0.802 for pristine counterparts.

Additionally, the current in forward biased Schottky diodes typically follow thermionic-emission equation.

$$I = A\,A^*T^2\,exp\left(\frac{-q\Phi_b}{kT}\right)\exp\left(\frac{qV}{nkT}\right)$$

Where A represents diode area, A* is the Richardson constant, T is the absolute temperature, q is the elementary charge, Φ_b is the barrier height, k is Boltzmann's constant, and V is the applied forward bias voltage, n is ideality factor which varies with V.

Furthermore, V_{oc} also directly related with built-in potential (V_{bi}) [44, 45]. Capacitance-voltage (C−V) measurements are used to study the electronic performance of both devices, and the plotting of $1/C^2$ −V (Fig. 6a) extrapolation to the abscissa can yield V_{bi}. Interface modified device demonstrate high V_{bi} value resulted an enhancement of V_{oc} [46]. The Al_2O_3-treated device produces a large internal electric field and a higher V_{bi}, leading to a wider depletion region. This, in turn, facilitates effective charge separation, thereby boosting the PCE. The heterojunction properties inherent to the Si/PEDOT device vary not only with the substrate's preconditioning and the atmospheric humidity during preparation but also with the time elapsed until measurement.

To study in-depth the junction of both devices, EIS measurements were carried out under dark conditions in a frequency range of 1 Hz–1MHz as shown in Fig. 6b. The impedance spectra comprise of semicircle which demonstrates a single junction for HSCs [47, 48]. The EIS-fitted circuit consists of recombination resistance (R_{rec}), series resistance (R_s), and junction capacitance (C_{jun}) [49]. Larger the diameter of a semicircle higher its resistance against R_{rec} and vice versa [50]. The interface-modified device shows a larger semicircle diameter compared to the native oxide, indicating an effective suppression of the charge recombination rate. Table 3 provide the values of R_s, C_{jun} and R_{rec} for both the interface-modified and native oxide devices.

Additionally, from the values of C_{jun} and R_{rec} minority carrier lifetime (τ) can be calculated using the following equation [46, 51].

$$\tau = R_{rec} \times C_{jun} \quad (3)$$

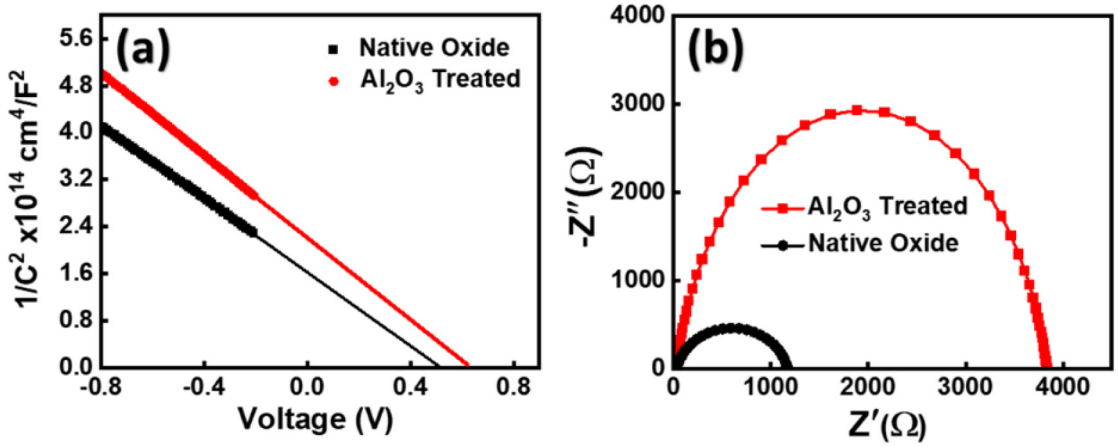

Fig. 6. (a) Capacitance-voltage (1/C−V) measurement and (b) Nyquist plot of structured Si/PEDOT:PSS.

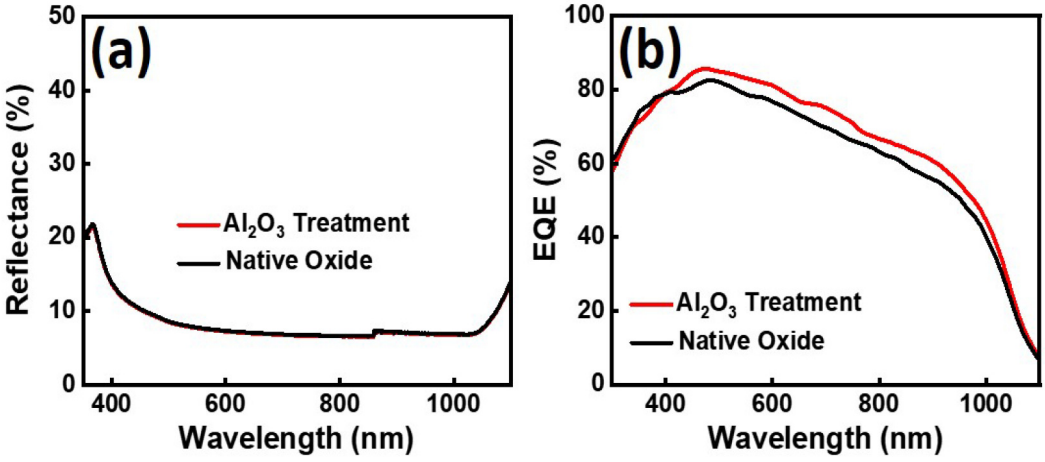

Fig. 7. (a) Comparison of the (a) spectral reflection and (b) EQE of the HSCs with and without interface modification.

Table 3. Impedance characteristics of the investigated devices.

Devices	R_s (ohm)	R_{rec} (ohm)	C_{Jun} (F)	Lifetime (μs)
Native Oxide	3.34	1170	1.79×10^{-8}	20.9
Al_2O_3 Treatment	2.29	3830	1.63×10^{-8}	62.4

The corresponding τ values are presented in Table 3. Additionally, τ values and enhanced performance of the HSCs matching well. Additionally, we performed reflectance and EQE analysis to evaluate the role of Al_2O_3 ultra-thin layer on the performance of HSCs. since both devices demonstrate same reflectance as shown in Fig. 7a [52]. Both devices absorbed same amount of photon is shown in Fig. 7a, the enhanced EQE (Fig. 7b) directly related with effective passivation at the front junction between structured Si and PEDOT:PSS mainly due to Al_2O_3 ultra-thin layer insertion which in turn minimizes the recombination of photogenerated charge carriers to enhanced the EQE.

4. Conclusion

In summary, we have successfully demonstrated the fabrication of high-efficiency heterojunction solar cells (HSCs) based on structured n-Si and PEDOT:PSS with insertion of uniform, and ultra-thin Al_2O_3 layer on front interface effectively suppressing the interfacial charge recombination and facilitate hole migration. Additionally, the Al_2O_3 thin layer provides better wettability of PEDOT:PSS compared to native oxide, which minimizes pores, and pin-hole density usually occurs in spin-coating process. The optimized HSCs exhibit a remarkable PCE of 14.3% alongside a high V_{oc} of 0.612 V. These results suggest a favorable method for the achievement of next-generation structured silicon/organic HSCs.

Conflict of interest

The authors declare no conflict of interest.

Author contribution

Sameer Alghanmi was responsible for writing the manuscript, visualization, and software analysis. Khalid Alshammari reviewed the paper, supervised the work, and participated in the analysis.

Data availability

The authors confirm that the data supporting the findings of this study are available within the article [and/or] its supplementary materials.

References

1. Al-Ezzi AS, Ansari MNM. Photovoltaic solar cells: A review. Applied System Innovation. Aug. 2022;5(4):4. doi: 10.3390/asi5040067.
2. Chuchvaga N, Zholdybayev K, Aimaganbetov K, Zhantuarov S, Serikkanov A. Development of hetero-junction silicon solar cells with intrinsic thin layer: A review. Coatings. Apr. 2023;13(4):4. doi: 10.3390/coatings13040796.
3. Zhang X *et al.* Improved PEDOT:PSS/c-Si hybrid solar cell using inverted structure and effective passivation. Sci Rep. Oct. 2016;6(1):1. doi: 10.1038/srep35091.
4. Ullah F, Hasrat K, Iqbal S, Wang S. Design and development of D-A-D organic material for solution-processed organic/Si hybrid solar cells with 17.5% power conversion efficiency. Molecules. Jan. 2024;29(22):22. doi: 10.3390/molecules29225369.

5. Ullah F, Hasrat K, Iqbal S, Wang S. Achieving 15.75% efficiency in solar cells: Advanced surface engineering using Tetra-Tert-Butyl-Tercarbazol-Benzonitrile and organic layer integration in n-type silicon wafer and hybrid Planar-Si systems. Solid-State Electronics. Jan. 2025;223:109025. doi: 10.1016/j.sse.2024.109025.
6. Zielke D, Pazidis A, Werner F, Schmidt J. Organic-silicon heterojunction solar cells on n-type silicon wafers: The BackPEDOT concept. Solar Energy Materials and Solar Cells. Dec. 2014;131:110–116. doi: 10.1016/j.solmat.2014.05.022.
7. Ali G, Shinde SS, Sami A, Kim S, Wagh NK, Lee J-H. Effect of interfacial passivation on inverted pyramid silicon/poly(3,4-ethylenedioxythiophene):Poly(styrenesulfonate) heterojunction solar cells. Thin Solid Films. Sep. 2020;709:138139. doi: 10.1016/j.tsf.2020.138139.
8. Li C *et al.* Performance Improvement of PEDOT:PSS/N-Si heterojunction solar cells by alkaline etching. Silicon. Mar. 2021. doi: 10.1007/s12633-021-01034-2.
9. Mu X *et al.* High efficiency organic/silicon hybrid solar cells with doping-free selective emitter structure induced by a WO_3 thin interlayer. Nano Energy. Sep. 2015;16:54–61. doi: 10.1016/j.nanoen.2015.06.015.
10. Punia U, Kumari P, Sharma RK, Laxmi S, Srivastava R, Srivastava SK. Fabrication of low-cost and efficient PEDOT:PSS-silicon hybrid heterojunction solar cell via tailoring the organic layer thickness. J Mater Sci: Mater Electron. Dec. 2023;35(1):42. doi: 10.1007/s10854-023-11812-w.
11. Zhang J, Meng K, Ni G. Enhanced lateral photovoltaic effects in n-Si/SiO2/PEDOT:PSS structures. Polymers. Jan. 2022;14(7):7. doi: 10.3390/polym14071429.
12. Zhou W *et al.* High conductivity PEDOT:PSS thin films affording improved open circuit voltages in PEDOT:PSS-Si heterojunction solar cells. Materials Letters. Apr. 2022;312:131466. doi: 10.1016/j.matlet.2021.131466.
13. Kumari P, Punia U, Sharma D, Srivastava A, Srivastava SK. Enhanced photovoltaic performance of PEDOT:PSS/Si heterojunction solar cell with ZnO BSF Layer: A simulation study using SCAPS-1D. Silicon. Apr. 2023;15(5):2099–2112. doi: 10.1007/s12633-022-02163-y.
14. Yang Y *et al.* Boost organic-silicon hybrid solar cell performances with a facile and cost-effective Sub-3 nm interface control method. Solar RRL. 2023;7(24)2300627. doi: 10.1002/solr.202300627.
15. Lu Z, Hou G, Zhu Y, Chen J, Xu J, Chen K. High efficiency organic–Si hybrid solar cells with a one-dimensional CdS interlayer. Nanoscale. Feb. 2021;13(7):4206–4212. doi: 10.1039/D0NR09122G.
16. Zhang G *et al.* Improving the performance of Si/PEDOT:PSS hybrid solar cells with more economical and environmentally friendly alcohol ether solvents. ACS Omega. Apr. 2024;9(13):15040–15051. doi: 10.1021/acsomega.3c09187.
17. Liu H *et al.* Effects of different interface on the stability of hybrid heterojunction solar cells. Solar Energy Materials and Solar Cells. Jan. 2024;264:112624. doi: 10.1016/j.solmat.2023.112624.
18. Tevi T, Saint Birch SW, Thomas SW, Takshi A. Effect of Triton X-100 on the double layer capacitance and conductivity of poly(3,4-ethylenedioxythiophene):poly(styrenesulfonate) (PEDOT:PSS) films. Synthetic Metals. May 2014;191:59–65. doi: 10.1016/j.synthmet.2014.02.005.
19. Vosgueritchian M, Lipomi DJ, Bao Z. Highly conductive and transparent PEDOT:PSS films with a fluorosurfactant for stretchable and flexible transparent electrodes. Advanced Functional Materials. 2012;22(2):421–428. doi: 10.1002/adfm.201101775.
20. Alamer FA *et al.* Review on PEDOT:PSS-based conductive fabric. ACS Omega. Oct. 2022;7(40):35371–35386. doi: 10.1021/acsomega.2c01834.
21. He L, Jiang C, Wang H, Lai D, Rusli. High efficiency planar Si/organic heterojunction hybrid solar cells. Applied Physics Letters Feb. 2012;100(7):073503. doi: 10.1063/1.3684872.
22. Zhang C, Zhang Y, Guo H, Jiang Q, Dong P, Zhang C. Efficient planar hybrid n-Si/PEDOT:PSS solar cells with power conversion efficiency up to 13.31% achieved by controlling the SiO_x interlayer. Energies. Jun. 2018;11(6):6. doi: 10.3390/en11061397.
23. Hasrat K *et al.* Fabrication of an organic/inorganic silicon hybrid solar cell based on PEDOT:PSS doped and non-doped with CBP and dibenzothiopene-benzoyl-tertiarybutylcarbozole. J. Electron. Mater. Mar. 2022;51(3):1342–1348. doi: 10.1007/s11664-021-09370-0.
24. Ullah F, Hasrat K, Iqbal S, Wang S. Optimizing solar cell performance: Hybrid planar-Si/organic heterojunction solar cells achieve 14.75% efficiency through dibenzothiophene-spirobifluorene-dithienothiophene insertion layer integration. Energy Technology. 2401249. doi: 10.1002/ente.202401249.
25. Ullah F *et al.* PEDOT: PSS/PC71BM with various Rubrene doping levels for the production of organic/inorganic hybrid silicon solar cells with enhanced yield efficiency. Materials Science and Engineering: B. Oct. 2024;308:117552. doi: 10.1016/j.mseb.2024.117552.
26. Sheng J *et al.* Improvement of the SiO_x passivation layer for high-efficiency Si/PEDOT:PSS heterojunction solar cells. ACS Appl. Mater. Interfaces. Sep. 2014;6(18):16027–16034. doi: 10.1021/am503949g.
27. Chen T, Guo H, Yu L, Sun T, Yang Y. Silicon substrate treated with diluted NaOH aqueous for Si/PEDOT: PSS heterojunction solar cell with performance enhancement. Energies. 2020;13(18):1–10.
28. Liu Y *et al.* Low-temperature synthesis TiOx passivation layer for organic-silicon heterojunction solar cell with a high open-circuit voltage. Nano Energy. Apr. 2017;34:257–263. doi: 10.1016/j.nanoen.2017.02.024.
29. Oke JA, Jen T-C. Atomic layer deposition and other thin film deposition techniques: from principles to film properties. Journal of Materials Research and Technology. Nov. 2022;21:2481–2514. doi: 10.1016/j.jmrt.2022.10.064.
30. Sardar W *et al.* Effect of ultra-thin ZnS passivation using ALD technique on the performance of heterojunction solar cells. Optical Materials. Nov. 2024:116375. doi: 10.1016/j.optmat.2024.116375.
31. Sharma RK *et al.* Graphene oxide modified PEDOT:PSS as an efficient hole transport layer for enhanced performance of hybrid silicon solar cells. Surfaces and Interfaces. Feb. 2023;36:102577. doi: 10.1016/j.surfin.2022.102577.
32. Qiu J *et al.* Enhanced efficiency of graphene-silicon Schottky junction solar cell through inverted pyramid arrays texturation. Journal of Materials Science & Technology. Nov. 2018;34(11):2197–2204. doi: 10.1016/j.jmst.2018.04.008.
33. Donoval M *et al.* Relation between secondary doping and phase separation in PEDOT:PSS films. Applied Surface Science. Feb. 2017;395:86–91. doi: 10.1016/j.apsusc.2016.05.076.
34. Iatsunskyi I, Kempiński M, Jancelewicz M, Załęski K, Jurga S, Smyntyna V. Structural and XPS characterization of ALD Al_2O_3 coated porous silicon. Vacuum. Mar. 2015;113:52–58. doi: 10.1016/j.vacuum.2014.12.015.
35. Nam Y-H *et al.* Planar n-Si/PEDOT:PSS hybrid heterojunction solar cells utilizing functionalized carbon nanoparticles

synthesized via simple pyrolysis route. Nanotechnology. Oct. 2017;28(47):475402. doi: 10.1088/1361-6528/aa9014.
36. Werner F *et al.* Electronic and chemical properties of the c-Si/Al_2O_3 interface. Journal of Applied Physics. Jun. 2011;109(11):113701. doi: 10.1063/1.3587227.
37. Pudasaini PR, Ruiz-Zepeda F, Sharma M, Elam D, Ponce A, Ayon AA. High efficiency hybrid silicon nanopillar–polymer solar cells. ACS Appl. Mater. Interfaces. Oct. 2013;5(19):9620–9627. doi: 10.1021/am402598j.
38. Yang L *et al.* Interface engineering of high efficiency organic-silicon heterojunction solar cells. ACS Appl. Mater. Interfaces. Jan. 2016;8(1):26–30. doi: 10.1021/acsami.5b10959.
39. He J *et al.* High-efficiency silicon/organic heterojunction solar cells with improved junction quality and interface passivation. ACS Nano. Dec. 2016;10)12):11525–11531. doi: 10.1021/acsnano.6b07511.
40. Mamykin SV, Lunko TS, Mamontova IB, Kondratenko OS, Berezovska NI, Romanyuk VR. Interface texturing for enhanced PEDOT:PSS/si solar cell efficiency. Molecular Crystals and Liquid Crystals. May 2024;768(7):34–42. doi: 10.1080/15421406.2024.2348176.
41. Das PK, Dhawan A. Plasmonic enhancement of photovoltaic characteristics of organic solar cells by employing parabola nanostructures at the back of the solar cell. RSC Advances. 2023;13(38):26780–26792. doi: 10.1039/D3RA03637E.
42. Hong L *et al.* 18.5% efficiency organic solar cells with a hybrid planar/bulk heterojunction. Advanced Materials. 2021;33(43):2103091. doi: 10.1002/adma.202103091.
43. Nam Y-H, Song J-W, Park M-J, Sami A, Lee J-H. Ultrathin Al2O3 interface achieving an 11.46% efficiency in planar n-Si/PEDOT:PSS hybrid solar cells. Nanotechnology. Mar. 2017;28(15):155402. doi: 10.1088/1361-6528/aa63b9.
44. Srivastava A, Sharma RK, Sharma D, Tawale JS, Agrawal VV, Srivastava SK. Unveiling the role of ethylene glycol for enhanced performance of PEDOT:PSS/silicon hybrid solar cells. Optical Materials. Dec. 2022;134:112922. doi: 10.1016/j.optmat.2022.112922.
45. Ahmmed S, Aktar A, Md. Ismail AB. Role of a solution-processed V_2O_5 hole extracting layer on the performance of CuO-ZnO-based solar cells. ACS Omega. May 2021;6(19):12631–12639. doi: 10.1021/acsomega.1c00678.
46. Nam Y-H *et al.* Planar n-Si/PEDOT:PSS hybrid heterojunction solar cells utilizing functionalized carbon nanoparticles synthesized via simple pyrolysis route. Nanotechnology. Oct. 2017;28(47):475402. doi: 10.1088/1361-6528/aa9014.
47. Lin G *et al.* Research progress in improving the performance of PEDOT:PSS/micro- and Nano-textured Si heterojunction for hybrid solar cells. Journal of Materiomics. Sep. 2021;7(5):1161–1179. doi: 10.1016/j.jmat.2020.12.013.
48. Khan J *et al.* Quantum-dot sensitized hierarchical NiO p–n heterojunction for effective photocatalytic performance. RSC Adv. Nov. 2022;12(50):32459–32470. doi: 10.1039/D2RA05657G.
49. Malik A, Muhyuddin M, Ali G, Wadood A, Tauqir A, Basit MA. Bi-efficacious incorporation of Indium in TiO_2/PbS based nanocomposites for photocatalytic and solar paint applications. Solar Energy. Nov. 2021;228:216–225. doi: 10.1016/j.solener.2021.09.057.
50. Ali G, Jazib Abbas Zaidi S, Abdul Basit M, Park TJ. Synergetic performance of systematically designed g-C_3N_4/rGO/SnO_2 nanocomposite for photodegradation of Rhodamine-B dye. Applied Surface Science. Dec. 2021;570:151140. doi: 10.1016/j.apsusc.2021.151140.
51. Wu W-Q, Xu Y-F, Su C-Y, Kuang D-B. Ultra-long anatase TiO_2 nanowire arrays with multi-layered configuration on FTO glass for high-efficiency dye-sensitized solar cells. Energy Environ. Sci. Jan. 2014;7(2):644–649. doi: 10.1039/C3EE42167H.
52. Trinh PV *et al.* Enhanced power conversion efficiency of an n-Si/PEDOT:PSS hybrid solar cell using nanostructured silicon and gold nanoparticles. RSC Adv. Mar. 2022;12(17):10514–10521. doi: 10.1039/D2RA01246D.